



Green Hydrogen Evolution Using Metal Active Center Electrocatalysts Stabilized by N-Doped Carbon Scaffolds

Izadora F. Reis,^{1,2}* Gabriel A. Diab,¹ Luis F.G. Noleto,¹ Bruna R. Serino¹, Ivo F. Teixeira,¹ Pablo J. Calvo²

Resumo/Abstract

RESUMO - Materiais de carbono dopados com nitrogênio têm se destacado como eletrocatalisadores promissores para a produção sustentável de hidrogênio, devido à sua estrutura modificável e abundância de sítios ativos. Neste trabalho, foi desenvolvido um carbono dopado com nitrogênio e sódio (Na-NC), posteriormente modificado por troca catiônica com metais (Ni, Mg, Fe, Co e Cu). Entre os catalisadores, o Co-NC apresentou o melhor desempenho na reação de evolução de hidrogênio (HER) em meio alcalino, com início de reação em -0,78 V vs RHE e densidade de corrente de -30 mA cm⁻² a -0,9 V vs RHE. Esse desempenho foi associado a propriedades como baixa resistência à transferência de carga, menor inclinação de Tafel e boa dispersão dos aglomerados de cobalto, confirmadas por análise STEM. Todos os compósitos mostraram bandas C–C típicas no FTIR, múltiplas etapas de decomposição no TGA e um pico largo em 27° no DRX, indicativo de estrutura amorfa grafítica. A troca catiônica mostrou-se uma abordagem simples e eficaz para melhorar a atividade catalítica de materiais à base de carbono dopado, com potencial aplicação em outras reações energéticas.

Palavras-chave: Carbono dopado com nitrogênio, Cobalto, Eletrocatalisadores, Hidrogênio verde.

ABSTRACT - In the pursuit of sustainable hydrogen production, nitrogen-doped carbon materials have emerged as promising electrocatalysts due to their tunable structure and abundant active sites. This study reports the synthesis of a sodium-based nitrogen-doped carbon (Na-NC) and its modification via metal cation exchange (Ni, Mg, Fe, Co, and Cu). Among the resulting catalysts, Co-NC showed the earliest onset potential (-0.78 V vs RHE) and highest current density (-30 mA cm⁻² at -0.9 V vs RHE) for alkaline HER. Multiple analyses were performed to determine key properties. For Co-NC, linear correlations indicated the lowest charge transfer resistance, smallest Tafel slope (faster kinetics), and well-dispersed Co clusters, confirmed by STEM elemental mapping. All composites showed typical C-C vibrational modes in FTIR and multi-step decomposition in TGA. XRD revealed a broad peak at 27°, consistent with an amorphous graphitic structure. Compared to Na-NC, metal exchange improved HER activity, suggesting that cation exchange is a simple and versatile method to enhance NC-based materials. The materials show promising electrochemical activity applicable to other energy-related reactions.

Keywords: Nitrogen-doped carbon, Cobalt, Electrocatalysts, Green hydrogen.

Introduction

In response to the urgent demand for sustainable hydrogen technologies, particularly production through electrochemical water splitting, recent research has focused on the development of cost-effective alternatives to noblemetal-based electrocatalysts for the hydrogen evolution reaction (HER). While noble metals such as platinum demonstrate outstanding catalytic activity, their high cost significantly limit their scarcity practical applications.(1-3) To address this challenge, nitrogen-doped carbon (N-doped carbon) materials have garnered increasing attention as promising support due to their excellent electrical conductivity, chemical stability in both acidic and alkaline media, and tunable surface properties.(4, 5)

Nitrogen doping plays a crucial role in modulating the electronic structure of carbon, introducing active sites that can enhance catalytic performance. However, N-doped carbon alone often falls short in delivering the desired HER activity. (6, 7) To improve efficiency, a novel approach has been employed in which low-cost transition metals are incorporated into the N-doped carbon framework via a simple ion exchange process. (8, 9) This method enables the formation of metal-N-C configurations, where the synergistic interactions between the metal centers and the nitrogen functionalities enhance the overall electrocatalytic activity. This strategy offers several advantages: it leverages

^{*}izadorafonseca@ufscar.br

¹Univerdade Federal de São Carlos (UFSCAR) - Departamento de Química, Brasil, UFSCar,

²Friedrich-Alexander-Universität Erlangen-Nürnberg (FAU) - Department of Chemistry and Pharmacy, Germany



earth-abundant and inexpensive metals, reduces the reliance on scarce noble metals, and allows for scalable synthesis. (10, 11) The simplicity and versatility of the ion exchange technique also enable the incorporation of a wide range of metals, providing opportunities for systematic exploration and optimization. (12) The ongoing research aims to evaluate various combinations of metals with N-doped carbon supports to identify efficient, stable, and economically viable HER electrocatalysts for sustainable hydrogen production. (13-15)

Experimental

Synthesis of Na-NC and ion exchange

The synthesis of nitrogen-doped carbon (NC) material began with the thermal treatment of a carbon source (e.g., cellulose) and sodium chloride (1:10 mass ratio), combined with hydrolyzed collagen (5 wt%) or another nitrogen source. The mixture underwent pyrolysis in a muffle furnace at 400 °C for 2 hours (heating rate: 5 °C/min) under a nitrogen atmosphere. After cooling to room temperature, the resulting product was purified by repeated washing with distilled water, filtration, and 24-hour sonication. The final material was then centrifuged and dried, yielding the Na-NC standard material. (16, 17)

To incorporate isolated transition metal atoms into the NC matrix, a previously developed ion exchange method was employed. Aqueous suspensions of the Na-NC material were mixed with different metal chlorides (e.g., Mg²⁺, Ni²⁺, Fe²⁺, Co²⁺, and Cu²⁺) in a 1:2 metal/Na-NC mass ratio. The suspension was then sonicated for 5 minutes and magnetically stirred for 1 hour at room temperature. The resulting mixtures were purified through Milli-Q water washing and drying. (18, 19) Figure 1: Schematic representation of the steps to obtain M-N-doped carbon. Figure 1 illustrates the steps involved in both the synthesis of the nitrogen-doped carbon material and the subsequent cation exchange process.

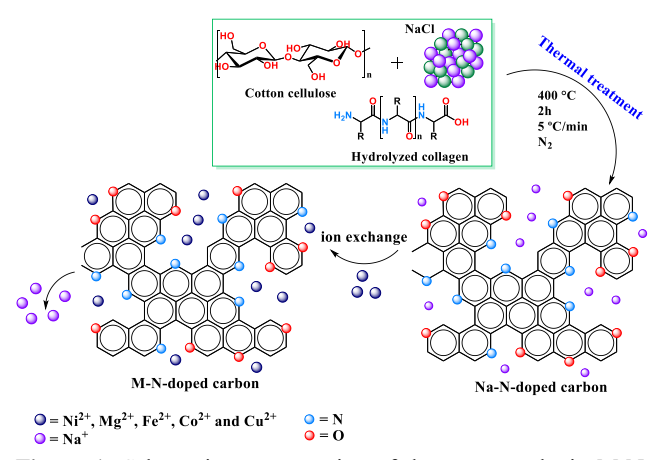


Figure 1: Schematic representation of the steps to obtain M-N-doped carbon.



Fabrication of carbon electrodes

Thin films were prepared in two steps: ionomer catalyst solution using perfluorosulfonic acid (PFSA) as a binder, and deposition on a Glassy Carbon Electrode (GCE) by drop casting, with 5 µL of the ink deposited on the electrode surface. The ink preparation consisted of 6 mg of the catalyst, 10 mL of PFSA, and 210 mL of ethanol, followed by drying for 30 minutes at room temperature. The electrochemical experiments were conducted in an alkaline electrolyte (0.1 mol L-1 KOH, pH 13). Linear sweep voltammetry (LSV) was performed in a potential range of -0.967 V to -1.967 V with a scan rate of 30 mV/s and step size of 1 mV. The sample area was 0.071 cm², and the open circuit potential was -0.219 V. Electrochemical impedance spectroscopy (EIS) measurements were carried out using a potentiostat in galvanostatic mode. The frequency range was set from 10⁵ Hz to 10⁻² Hz, with 10 points per decade. The AC current amplitude was 10 µA, and the sample area was 0.071 cm². The experiments were conducted under open circuit conditions at a potential of -0.125 V.

Materials characterization

All synthesized materials were characterized by thermogravimetric analysis (TGA) to assess their thermal stability. Structural properties were investigated using X-ray diffraction (XRD), while functional groups were identified by Fourier-transform infrared spectroscopy (FTIR). Morphological analysis was carried out by transmission electron microscopy (STEM), specifically for Na-NC and Co-NC.

Results

Electrochemical performance

The composites were evaluated through electrochemical performance to study the impact of different incorporated metals towards hydrogen production. The latter was possible due to linear sweep voltammetry (LSV) measurements (Figure 2). Among the catalysts tested, Co-NC exhibited the highest activity, achieving a current density of 30 mA.cm⁻² at -0.9 V vs RHE, which reflects its enhanced proton reduction kinetics. The onset potentials depended on the metal incorporated: Cu-NC at -0.90 V, Fe-NC at -0.83 V, Ni-NC at -0.78 V, and Co-NC at -0.70 V, all vs. RHE. Co-NC displayed the most favorable onset potential, highlighting its superior electrocatalytic performance. In contrast, Na-NC and Mg-NC exhibited no activity for hydrogen production.

The superior activity of Co-NC may be attributed to cobalt's favorable electronic structure, which facilitates more



efficient charge transfer and proton adsorption in the solidliquid interface.(20)

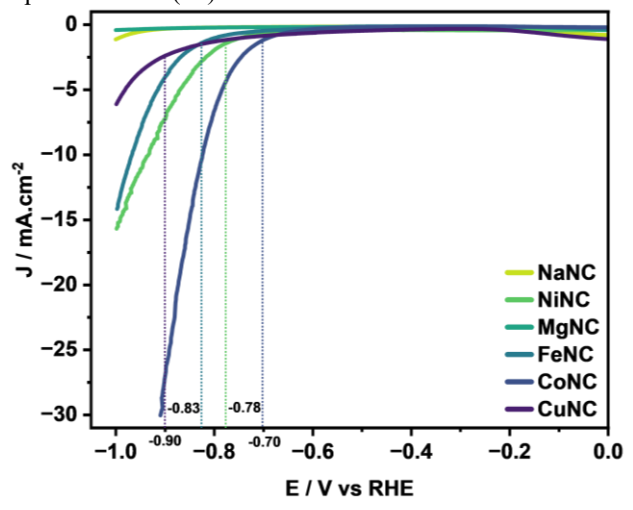


Figure 2: HER polarization curves for Na-NC and M-NC composites (M = Ni, Mg, Fe, Co, and Cu) electrodes.

Tafel slope analysis (Figure 3) further confirms the electrocatalytic activity of the materials. Co-NC exhibited the lowest Tafel slope at 128 mV.dec⁻¹, indicating the most favorable kinetics among the tested composites. Na-NC, Ni-NC, Fe-NC, and Cu-NC followed with values of 151, 163, 179, and 222 mV.dec⁻¹, respectively. In contrast, Mg-NC showed a significantly higher slope of 593 mV.dec⁻¹, reflecting poor electrocatalytic efficiency.

All materials, except for Mg-NC, exhibited Tafel slopes around or slightly above 120 mV·dec⁻¹, suggesting that HER proceeds via the Volmer-Heyrovsky mechanism, with the proton adsorption step (Volmer) being rate-determining. The particularly low slope observed for Co-NC implies enhanced charge transfer and more accessible active sites. These findings reinforce the superior performance of Co-NC for HER.(21)



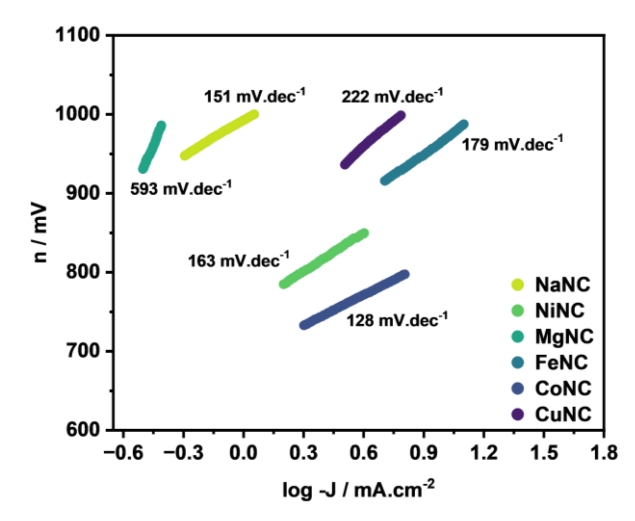


Figure 3: HER Tafel slopes for Na-NC and M-NC composites (M = Ni, Mg, Fe, Co, and Cu) electrodes.

Electrochemical impedance spectroscopy (EIS) via Nyquist plot (Figure 4) further supports the findings obtained from LSV and Tafel slope analysis, confirming that Co-NC exhibits the highest electrocatalytic activity, as evidenced by its lowest charge transfer resistance ($R_{\rm ct}$), i.e., 62 KOhm. This result aligns with the hypothesis that the presence of catalytically active sites enhances charge transport and facilitates proton adsorption during HER. In contrast, Mg-NC displays the highest $R_{\rm ct}$, reflecting high resistive contribution and thus poor conductivity – predominant factor for running efficiently electron flow in an electrochemical circuit. This possibly happens likely due to the absence of electrochemically useful active sites, capable of efficiently mediating the HER.

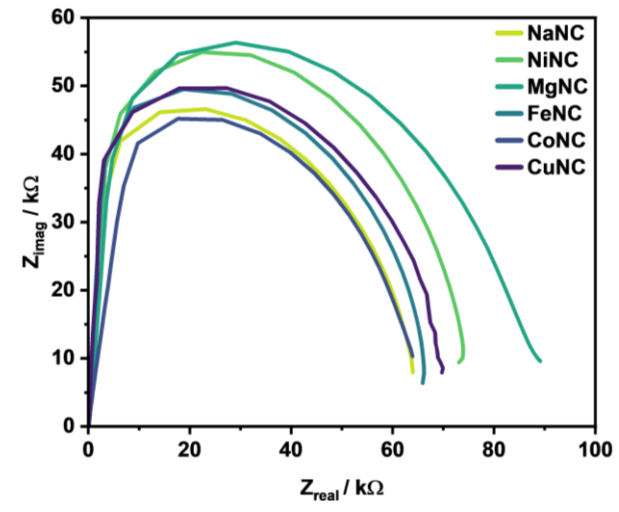


Figure 4: Nyquist plot for Na-NC and M-NC composites (M = Ni, Mg, Fe, Co, and Cu) electrodes.

Structural Characterization and Thermal Stability
Thermogravimetric analysis (TGA) provides the decomposition curves (Figure 5) of all composites,



revealing two distinct mass loss events in the samples. The first weight loss occurs below 100 °C and corresponds to the release of physically adsorbed water, weakly bound to the material. This process indicates a low water content, with less than 5% of the total mass. The materials remain thermally stable up to approximately 350 °C. Beyond this temperature, a continuous decomposition process begins, which proceeds until around 900 °C, where the residue stabilizes as a solid phase.

Importantly, all metal-incorporated samples exhibit similar thermal behavior, suggesting that the ion-exchange process did not compromise the structural integrity of the support. This consistency across different metals highlights the thermal robustness of the material, even after modification.

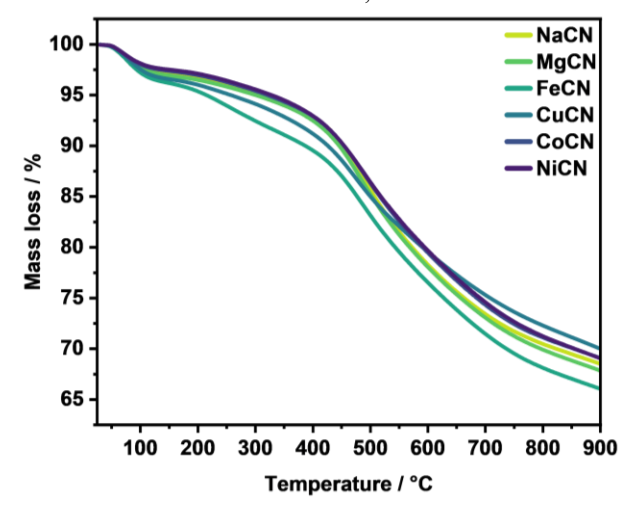


Figure 5: TGA results for Na-NC and M-NC composites (M = Ni, Mg, Fe, Co, and Cu).

Identifying the functional groups existing in the N-doped carbon is crucial to identifying the interaction nature between the transition metal and the support. Hence, Fourier Transform Infrared Spectroscopy (FT-IR) analyses were performed comparatively, Figure 6. Summarizing, bands associated to C-N, C-C, C=N and C=C are present and observed in the fingerprint region (window from 1000-1600 cm⁻¹). Additionally, a single and weak band related to C≡C bonds are seen at 2100 cm⁻¹. Foremost, the metal presence into the carbonaceous backbone can be observed around 1000 cm⁻¹, however, this signal is not selective to distinguish the interaction nature between nitrogenated or oxygenated sites. No loss of this band was detected across the transitions metal series.(17) Typically, signals attributed to stretching vibrations of C-H, O-H and N-H are observed. A comparative analysis between the spectra of the reference materials and the counterparts containing transition metals reveals no significant changes in the backbone of the support and neither additional bands formation.



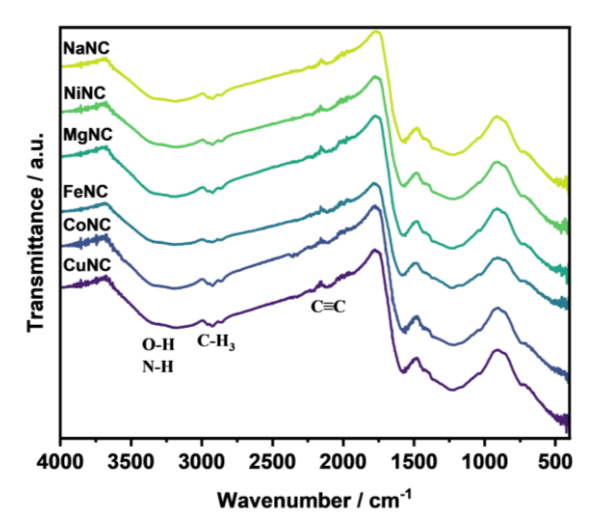


Figure 6: FT-IR spectra of Na-NC and M-NC composites (M = Ni, Mg, Fe, Co, and Cu).

The Powder X-Ray Diffraction (PXRD, Figure 7) pattern of N-doped materials aim to follow changes in the lattice after the cationic exchange. Given the broad nature of the peak that covers a large portion of the spectra (10 to 30°), all samples are considered to be amorphous. The main peak, with the maximum at 25° correspond to 002 reflection typical for carbonaceous amorphous matrices.(17). The same pattern is also observed for the materials containing transition metals, indicating the preservation of the lattice scaffold, even after the cation exchange process occurred. Especially for the sample containing Co, Figure 8, new diffraction peaks emerge which corroborate the Co(OH)₂ crystals formation but modified with Cl⁻ anions (22, 23), evidencing the nucleation of this second parasite phase.

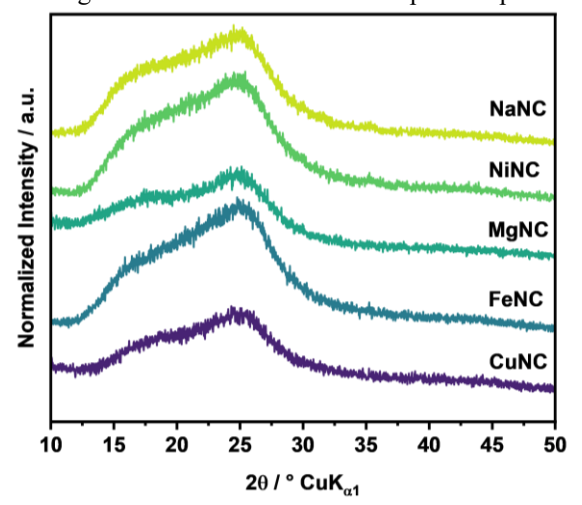


Figure 7: XRD patterns for Na-NC and M-NC composites (M = Ni, Mg, Fe, and Cu).



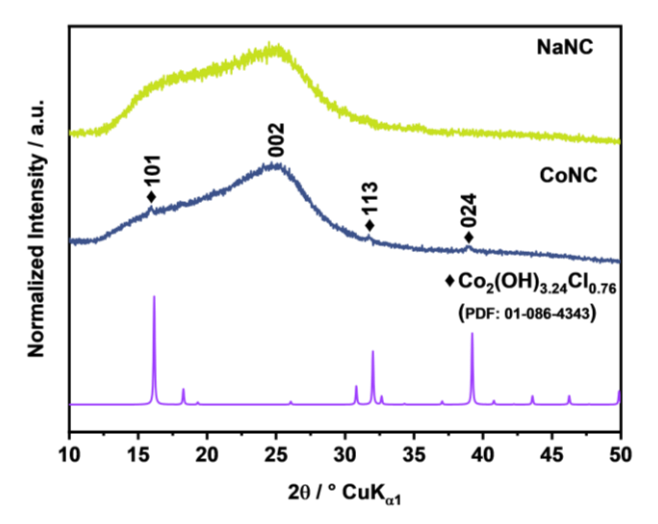


Figure 8: XRD patterns of Na-NC and Co-NC composites, as well as the Co₂(OH)_{3.24}Cl_{0.76} reference.

Morphological Analysis and Elemental Mapping
HAADF-STEM images (Figure 9, left) revealed a
morphology composed of stacked nanosheets shaping grain
of approximately 1 μm. Additionally, needle-like rod
structures were observed, which has been ascribed to cobalt
hydroxide (Co(OH)₂). Though the incorporation of
chlorides into the crystalline structure, the formation of
Co(OH)₂ ocurred as parasite phase. Elemental mapping by
EDS showed that cobalt (in red) is not only concentrated in
these needle-like regions but also homogeneously
distributed across the nitrogen-doped carbon matrix (in
blue). This indicates the coexistence of two distinct cobalt
species: crystalline Co(OH)₂ and atomically dispersed
cobalt, most likely coordinated with nitrogen and oxygen
functionalities within the carbon structure.

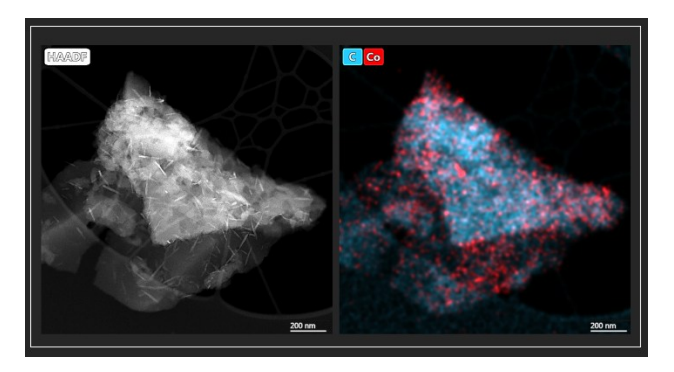


Figure 9: STEM-HAADF images of Co-NC composite (left) and EDS mapping (right).

Conclusion

This study demonstrates the potential of nitrogen-doped amorphous carbon stabilizing metal active centers. It has shown itself to be a versatile platform to coordinate single atoms. However, the host centers and chemical interactions



are still pending to be elucidated. Among the as-prepared electrocatalysts with different metal centers (Ni, Mg, Fe, Co, and Cu), Co-NC exhibited the earlier onset potential (-0.78 V vs RHE) and highest current density -30 mA cm⁻² at -0.9 V vs RHE when tested against alkaline HER. Linear correlations were found for Co-NC, for example it exhibited the lowest charge transfer resistance, lowest Tafel slope implying faster kinetics. Despite these promising results, it is still unclear which cobalt species, crystalline Co(OH₎₂ or atomically dispersed Co coordinated to N and O, or both, is responsible for the observed catalytic activity. The M-NC composite structure presents an attractive and transferable material strategy to be tested in several energy-related applications.

Acknowledgments

We acknowledge the FAPESP grant 2024/00839-5, CNPq 153749/2024-5, CAPES and FINEP. The chair "Chemistry of Thin Film Materials"- Energy NanoHybrid Interfaces' group of Friedrich-Alexander-Universität Erlangen, Germany.

References

- Y. Wang, H. Su, Y. He, L. Li, S. Zhu, H. Shen, P. Xie, X. Fu, G. Zhou, C. Feng, D. Zhao, F. Xiao, X. Zhu, Y. Zeng, M. Shao, S. Chen, G. Wu, J. Zeng, and C. Wang, Chemical Reviews 120, 12217 (2020).
- C. Wang, W. Guo, T. Chen, W. Lu, Z. Song, C. Yan, Y. Feng, F. Gao, X. Zhang, Y. Rao, L. Qian, S. Xu, G. Huang, Y. Zheng, W. Yan, and J. Zhang, *Coordination Chemistry Reviews* 514, 215899 (2024).
- 3. W. Zhang, R. Xi, Y. Li, Y. Zhang, P. Wang, and D. Hu, *International Journal of Hydrogen Energy* **47**, 32436 (2022).
- 4. C. Wang, Z. Wang, H. Wang, Y. Chi, M. Wang, D. Cheng, J. Zhang, C. Wu, and Z. Zhao, *International Journal of Hydrogen Energy* **46**, 9030 (2021).
- 5. Y. Yang, J. Su, P. Jiang, J. Chen, L. Hu, and Q. Chen, *Chinese Journal of Chemistry* **39**, 2626 (2021).
- 6. J. Yin, Q. Fan, Y. Li, F. Cheng, P. Zhou, P. Xi, and S. Sun, *Journal of the American Chemical Society* **138**, 14546 (2016).
- 7. W. Pei, S. Zhou, Y. Bai, and J. Zhao, *Carbon* **133**, 260 (2018).
- 8. Y. Zhu, J. Su, J. Liao, H. Peng, Z. Wang, Y. Wang, W. Wang, M. Luo, S. Li, and W. Li, *Next Materials* **6**, 100491 (2025).





- G. F. S. R. Rocha, M. A. R. da Silva, A. Rogolino, G. A. A. Diab, L. F. G. Noleto, M. Antonietti, and I. F. Teixeira, *Chemical Society Reviews* 52, 4878 (2023).
- 10. H. Hou, C. R. Bowen, D. Yang, and W. Yang, *Chem* **10**, 800 (2024).
- 11. J. Verma and S. Goel, *International Journal of Hydrogen Energy* **47**, 38964 (2022).
- 12. Z. Shi, W. Yang, Y. Gu, T. Liao, and Z. Sun, *Advanced Science* **7**, 2001069 (2020).
- M. L. M. Oliveira, C. M. A. C. Alves, C. F. Andrade, D. C. S. de Azevedo, F. L. Lobo, A. Fuerte, P. Ferreira-Aparicio, C. Caravaca, and R. X. Valenzuela, *ACS Omega* 10, 3282 (2025).
- 14. Z.-d. Wang, T. Xia, Z.-h. Li, and M.-f. Shao, *New Carbon Materials* **39**, 67 (2024).
- 15. M. A. Qadeer, X. Zhang, M. A. Farid, M. Tanveer, Y. Yan, S. Du, Z.-F. Huang, M. Tahir, and J.-J. Zou, *Journal of Power Sources* **613**, 234856 (2024).
- Z. Chen, A. Savateev, S. Pronkin, V. Papaefthimiou, C. Wolff, M. G. Willinger, E. Willinger, D. Neher, M. Antonietti, and D. Dontsova, *Advanced Materials* 29, 1700555 (2017).
- 17. W. V. F. do Carmo Batista, W. L. de Oliveira, E. F. de Oliveira, T. S. Cruz, J. L. Ferrari, B. S. Archanjo, S. Grigoletto, D. E. da Costa Ferreira, F. V. Pereira, G. A. A. Diab, V. R. Mastelaro, I. F. Teixeira, and J. P. de Mesquita, *ChemCatChem* 16, e202400400 (2024).
- M. A. R. da Silva, G. F. S. R. Rocha, G. A. A. Diab, C. S. Cunha, V. G. S. Pastana, and I. F. Teixeira, *Chemical Engineering Journal* 460, 141068 (2023).
- 19. A. A. Diab G, F. Reis I, Wang C, Barreto D, Savateev O, and F. T. I. ChemRxiv, 2025.
- H. Fei, Y. Yang, Z. Peng, G. Ruan, Q. Zhong, L. Li, E. L. G. Samuel, and J. M. Tour, ACS Applied Materials & Interfaces 7, 8083 (2015).
- 21. R. Sun, X. Huang, J. Jiang, W. Xu, S. Zhou, Y. Wei, M. Li, Y. Chen, and S. Han, *Dalton Transactions* 51, 15205 (2022).
- 22. P. M. De Wolff, Acta Crystallographica 6, 359 (1953).
- S.-H. Song, J. A. Alonso, M. T. Fernández-Díaz, and S. H. Lim, *European Journal of Inorganic Chemistry* 2017, 2289 (2017).